AIAA Propulsion and Energy Forum
August 9-11, 2021, VIRTUAL EVENT
AIAA Propulsion and Energy 2021 Forum

10.2514/6.2021-3529

Study of Direct Gas Injection into stagnation zone of Blunt Nose at Hypersonic Flow

Peter Harmon*, Ashish Vashishtha†, Dean Callaghan‡, and Cathal Nolan§
Institute of Technology Carlow, IRELAND, R93 V960

Ralf Deiterding¶
University of Southampton, Southampton, England SO17 1BJ, United Kingdom

Abstract

Direct gas injection in the shocked or compressed region has importance in many applications from drag control to ignition and pressure gain combustion. This numerical study is focused on direct light gas injection into the stagnation zone of a blunt nose at hypersonic speed, aiming to achieve efficient active drag control. The direct injection of a inert gas helium and a reactive gas hydrogen in the stagnation zone of bow-shock, are compared numerically with the air injection at hypersonic flow Mach 6 with freestream conditions according to the Earth's altitude of 10 km. The two-dimensional axisymmetric numerical simulations are performed by adaptive mesh refinement and solving compressible Euler equations for multiple thermally perfect species with a reactive source term using AMROC solver. The hydrogen combustion and ignition is modelled using one-step reaction mechanism. The pressure drag on the blunt nose has been compared for different injection pressure ratios for all three gas injections and it was concluded that the sonic injection (at Mach = 1) of light gases He and H_2 provides similar performance in the pressure drag reduction up to 77 %, as compared to air injection, with 62.5 % and 73.5 % lesser mass flow rate, respectively. In case of supersonic gas injection (at Mach = 2), the inert gas helium injection performs relatively better (up to 82 % pressure drag reduction) or comparable to supersonic air injection for lesser mass flow rates. Various flow features in the short and long penetration modes of sonic and supersonic gas injections are also analyzed in the reactive and non-reactive flow-fields.

Nomenclature

P	=	Pressure
U	=	Velocity
M	=	Mach Number
C_D	=	Drag Coefficient
d, D	=	Diameter
A	=	Cross-sectional Area
R_{MA}	=	Jet to Freestream Momentum Ratio
PR	=	Jet to Freestream Total Pressure Ratio
ρ	=	Density
$\dot{m}$	=	Mass flow rate
Subscripts	=	
∞	=	Freestream
j	=	Nozzle Exit Parameters
0	=	Total Conditions

*Joint First Author, Undergraduate Student, Aerospace & Mechanical Engineering, Institute of Technology Carlow, IRELAND.
†Joint First Author, Assistant Lecturer, Aerospace & Mechanical Engineering, Institute of Technology Carlow, IRELAND and AIAA Member.
‡Director, The Centre for Research and Enterprise in Engineering (engCORE), Institute of Technology Carlow, IRELAND.
§Head of Department, Aerospace, Mechanical and Electronics Engineering, Institute of Technology Carlow, IRELAND.
¶Associate Professor, Aerodynamics and Flight Mechanics Research Group, Highfield Campus, University of Southampton, UK.

I. Introduction

THE direct gas injection of reactive and non-reactive gases in supersonic or hypersonic stream may be used in various applications e.g. drag reduction by bow-shock manipulation near the injection point, counter thrust (drag increase) in retro-propulsion as well as shock induced ignition in scramjet engine or detonation initiation in non-premixed pressure gain combustion systems. In the area of aerodynamic heating mitigation and drag reduction at hypersonic flows, many studies [1] have been performed using various active and passive controls methods in order to manipulate the frontal bow-shock. Mechanical devices, such as a spike in front of a blunt nose can be used as a passive control method. In contrast, the flow-field associated with different lengths of a spike shows high unsteady fluctuations in hypersonic flow regimes[2, 3]. Breathing blunt nose is an another passive flow control method, which provides pressure relaxation in the stagnation zone and increase base pressure at supersonic[4] and hypersonic[5] flows. This technique has also limitation because of requirement of annular design, which can lead to higher weight. Frontal hemispherical cavity has also been considered effective passive control in hypersonic flows for drag increase and better heat transfer [6, 7]. The hemispherical cavity is also subjected to various non-stationary unsteady large and small amplitude fluctuations, which require an additional flow control methods to stabilize the flow field [8]. Among the various active flow control techniques, energy deposition methods by means of laser[9], microwave [10] or electric discharge[11] suffers from complicated energy source requirements. On the other hand, the counter-jet injection [1, 12, 13] has been found to be more practical in providing the required and on-demand drag reduction. Additionally, when a higher mass flow rate of gas is injected in front of the blunt nose, this system can also be adapted to slow down or drag increase [14]. Most of the studies with counter-jet injection are performed using air as injection gas. Among very few studies on injection of light gases[1], Vashishtha et al.[15] have performed numerical study of direct hydrogen injection in the stagnation zone and found that theoretically, the requirement of hydrogen mass flow rate is far lesser than required air to enable similar drag reduction. This means that the lighter gas injection may provide better performance in terms of drag reduction than compared to air injection of same mass flow rate. The direct hydrogen injection may also provide energy addition by self-ignition of hydrogen-air mixture with available high-pressure air in stagnation zone. In previous researches of counter-jet flows, two distinct flow behaviours named as short penetration mode (SPM) and long penetration modes (LPM) are observed, which are governed by the injection pressure, incoming flow condition as well injecting gas [16]. Long penetration mode (LPM) was found highly unsteady in nature and provide higher drag reduction, which pushes the bow-shock far upstream in comparison to short penetration mode (SPM). In the short penetration mode, the bow-shock deflects side-wards and provide low-pressure region in front of blunt nose by vortex formation. The hydrogen injection in short penetration mode leads to a standing flame between bow-shock and incoming hydrogen jet. The hydrogen direct injection for long penetration mode may push the bow-shock to higher upstream distances in comparison to air because of additional energy addition. In previous study by Vashishtha et. al [15], it was not conclusive whether the local detonation in stagnation zone can cause higher upstream shock movement while direct hydrogen injection. Overall, it was observed that the hydrogen injection in short penetration mode is comparable to air injection for drag reduction, but hydrogen injection in long penetration modes are highly effective in moving bow-shock away from the body, when compared to the air injection. Fundamentally, the effect of hydrogen injection can not be directly compared with air injection because of different mechanism of flow control by counter-jet as well as energy addition. Hence, the current study proposed direct injection of another light gas Helium, which will only provide momentum effect on bow-shock manipulation. In order to develop the understanding of drag control by light gas counter-jet injection, the effectiveness of helium, hydrogen and air injections have been studied numerically at hypersonic Mach number 6. The main motivation of this numerical study is to use high-pressure light gas injection as an effective active drag control technique for a blunt nose in hypersonic flows. However, the studies of direct hydrogen injection in the stagnation zone or the shocked air, can also be of interest for pressure gain combustion systems such as rotatory detonation engine operating at non-premixed mode [17]. High-pressure hydrogen gas injection in high pressure stagnation zone may provide the right conditions to initiate the pressure gain combustion mode. With the above two thoughts in the mind, this study proposes to study the effects of helium, hydrogen and air injection into stagnation zone of blunt nose at hypersonic flow. The Mach number of incoming hypersonic air is fixed as $M_\infty = 6$, with pressure and temperature conditions according to an altitude of 10 km in Earth's atmosphere. The sonic and supersonic air, helium and hydrogen gas injection simulation are performed at various jet to freestream stagnation pressure ratio (PR) conditions. The physics of non-reacting gas injection in counter-jet flow involves various interactions of frontal and reattached shockwaves, Mach disc, shear layers and re-circulation zones which can span from very small scale to scale of blunt nose. Further, the reactive gas injection, such as hydrogen will additionally involve small reaction and ignition zones. Hence, in this study dynamic Structured Adaptive Mesh Refinement (SAMR) based an open-source solver Adaptive Mesh Refinement Object-oriented C ++

(AMROC)[18] has been employed by solving axisymmetric unsteady compressible Euler's equations with multiple species and reactive source term. AMROC solver has been well established and validated for various multi-dimensional detonation [18–21] problems also, which makes it right choice for current parametric study. The overall objectives of this study are defined as: 1) to model and simulate air, helium and hydrogen injections in front of blunt nose at hypersonic speed using adaptive refinement based solver AMROC, 2) compare the effects of light gas (helium and hydrogen) injection on drag control, and 3) analyse the mode of combustion in case of hydrogen injection.

II. Numerical Method

The two-dimensional axisymmetric simulations are performed by solving unsteady multi-component compressible Euler equations with reaction source term as follows:

$$\frac{\partial \mathbf{U}}{\partial t} + \frac{\partial \mathbf{F}}{\partial x} + \frac{\partial \mathbf{G}}{\partial r} + \frac{\mathbf{Z}}{r} = \mathbf{S} \tag{1}$$

where conservative state vector **U**, flux vectors **F**, **G** and **Z** and source term **S** are defined below:

$$\mathbf{U} = \begin{Bmatrix} \rho_1 \\ \rho_2 \\ \vdots \\ \rho_n \\ \rho u \\ \rho v \\ e \end{Bmatrix}, \quad \mathbf{F} = \begin{Bmatrix} \rho_1 u \\ \rho_2 u \\ \vdots \\ \rho_n u \\ \rho u^2 + p \\ \rho uv \\ u(e+P) \end{Bmatrix}, \quad \mathbf{G} = \begin{Bmatrix} \rho_1 v \\ \rho_2 v \\ \vdots \\ \rho_n v \\ \rho v^2 + p \\ \rho uv \\ v(e+P) \end{Bmatrix}, \quad \mathbf{Z} = \begin{Bmatrix} \rho_1 v \\ \rho_2 v \\ \vdots \\ \rho_n v \\ \rho v^2 \\ \rho uv \\ v(e+P) \end{Bmatrix}, \quad \text{and} \quad \mathbf{S} = \begin{Bmatrix} \dot{\omega_1} \\ \dot{\omega_2} \\ \vdots \\ \dot{\omega_n} \\ 0 \\ 0 \\ 0 \end{Bmatrix} \tag{2}$$

Total Density:

$$\rho = \sum_{i=1}^{n} \rho_i \tag{3}$$

Energy:

$$e = \rho h - p + \frac{1}{2}\rho(u^2 + v^2) \tag{4}$$

Specific Enthalpy:

$$h = \sum_{i=1}^{n} \frac{\rho_i h_i}{\rho} \tag{5}$$

Equation of State:

$$p = \sum_{i=1}^{n} \rho_i \frac{R}{w_i} T \tag{6}$$

In the above equations, W_i is the molecular weight of each species, R is the universal gas constant and T is the local temperature. The source term $\dot{\omega}_i$ is the specific mass production rate of each species, which depends on the chemical reaction mechanism model:

$$\dot{\omega} = \sum_{j=1}^{M} (\nu'_{ji} - \nu^f_{ji}) \left[k^f_j \prod_{n=1}^{K} \left(\frac{\rho_n}{w_n} \right)^{\nu^f_{jn}} - k^r_j \prod_{n=1}^{K} \left(\frac{\rho_n}{w_n} \right)^{\nu^r_{jn}} \right], \quad i = 1, ..., K \tag{7}$$

The used solver module of AMROC [18] can use detailed chemical kinetics in Chemkin format[22], where the thermal and transport properties are evaluated based on NASA polynomial [23]. In the current study, the hydrogen-air combustion has been modelled using four species, single step hydrogen-air Arrhenius Kinetics [24]. Additional specie, the inert helium, is added in the Chemkin mechanism of single step chemistry. The forward or backward reaction rates are modelled with the following reaction coefficients:

$$k = AT^n exp\left(-\frac{E_a}{RT}\right) \tag{8}$$

where, $A = 2.25 \times 10^{18}\ cm^3 mol^{-1} s^{-1}$, $n = 0.0$ and $E_a = 17000\ cal/mol$. Helium is not present in any of the simulated cases, when hydrogen in injected and vice versa. The addition of helium properties allow the same solver module to be used for simulating hydrogen, helium and air (O_2:N_2 = 1:3.76) injection in stagnation zone. AMROC solver uses a time-operator splitting approach or method of fractional steps to decouple hydrodynamic transport and chemical reactions numerically [18]. In the current solver, Godunov splitting is adopted for decoupling and the second-order accurate MUSCL-TVD finite volume method (FVM) for the convective flux discretization [20]. A hybrid Roe-HLL Riemann solver is used for the construction of the inter-cell numerical upwind fluxes, while the Van-Albada limiter is applied with the MUSCL reconstruction to construct a second-order method in space. The second-order accurate MUSCL-Hancock technique is adopted for time integration. The dynamic time stepping is used for all simulations by keeping the CFL number 0.95. The structured adaptive mesh refinement (SAMR) method based on various flow parameters has been utilized here, which have lower numerical diffusion in highly refined regions. The following sections discuss about computational domain, boundary conditions and grid independence studies.

A. Computational Domain and Boundary Conditions

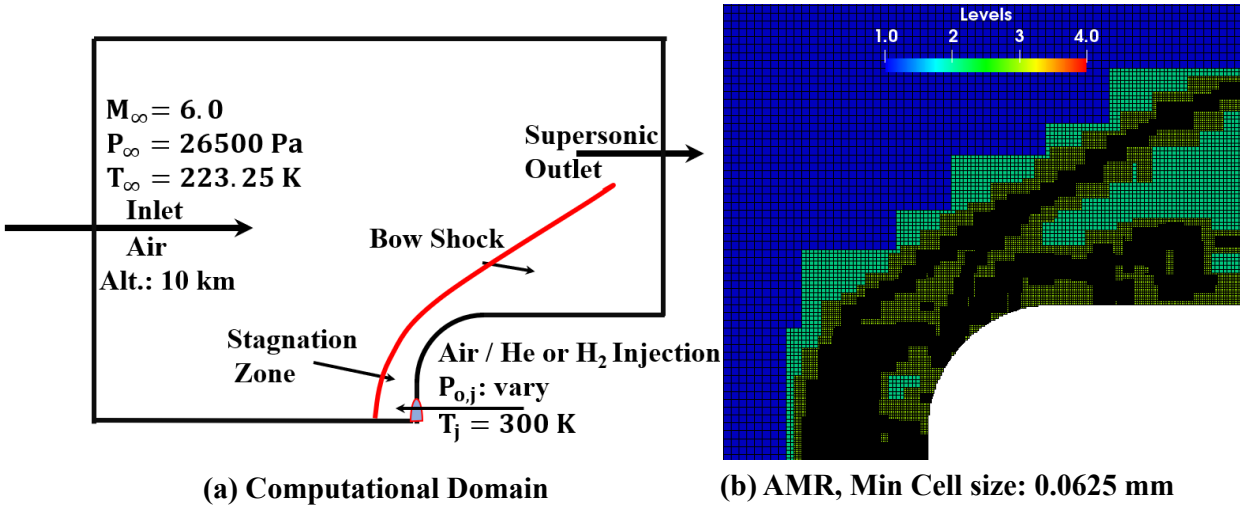

(a) Computational Domain **(b) AMR, Min Cell size: 0.0625 mm**

Fig. 1 (a) Computational Domain (b) Sample Grid refinement for air injection case

The computational domain consists of a 120 mm × 100 mm rectangular domain with a blunt nose of cross-section diameter 40 mm. The frontal section of blunt nose is modelled as a 4 mm radius flat surface to facilitate the counter-jet gas injection from a 2 mm radius hole. The shoulder of blunt nose has a 16 mm radius fillet. Figure 1a shows the schematic of computational domain with the free-stream inlet, gas injection inlet and outlet. The freestream inlet has been modelled as an incoming hypersonic Mach 6 air flow conditions at 10 km Earth's altitude, with static pressure and temperature as 26.5 kPa and 223.25 K, respectively. The bottom side before the blunt nose is modelled as axial symmetric. The top and the right side boundaries are considered as supersonic outlets. Slip and adiabatic wall boundary conditions are used for the blunt nose wall. The center region of 2 mm radius has been modelled as inlet for sonic and supersonic gas injection. The temperature of the injected gas was kept constant as 300 K, while the stagnation pressure of the counter-jet injection ($P_{0,j}$) is varied to control the injection strengths of different gases such as air, helium and hydrogen. The time-dependent computations are performed up to 10 ms, with an auto-adjusted time step based on an effective CFL number of 0.95. All the simulation cases are started with impulse start at $t = 0$ s with smaller initial velocity around the blunt nose. After the stable bow shock is established in front of the blunt nose for 1-2 ms duration, the counter-jet gas is injected at $t = 5$ ms. It will provide the sufficient time duration from $t = 5$ to 10 ms to analyze the flow-field of counter-jet flow gas injection. The base resolution of 1 mm × 1 mm has been used for all the computed cases. AMROC uses time-dependent block structured adaptive mesh refinement (SAMR) method[18], where the zones for mesh adaptation can be flagged with the defined parameters and different levels of refinements can be used as shown in Fig. 1b. The current study requires resolution of various interactions of shockwaves, shear layer in non-reacting air counter-jet flow, additionally interaction and mixing of different density gases in helium counter-jet flow and finally reaction and self-ignition zone resolution for hydrogen counter-jet flow. In AMR approach the adaptation of cells are

based on flagging with thresholds of density, pressure and temperature. The threshold values for temperature, density and pressure used are $\varepsilon_T = 5 \times 10^2$, $\varepsilon_\rho = 5 \times 10^{-2}$, and $\varepsilon_P = 9 \times 10^4$, respectively for all the cases.

B. Grid Independence in Non-Reactive Case

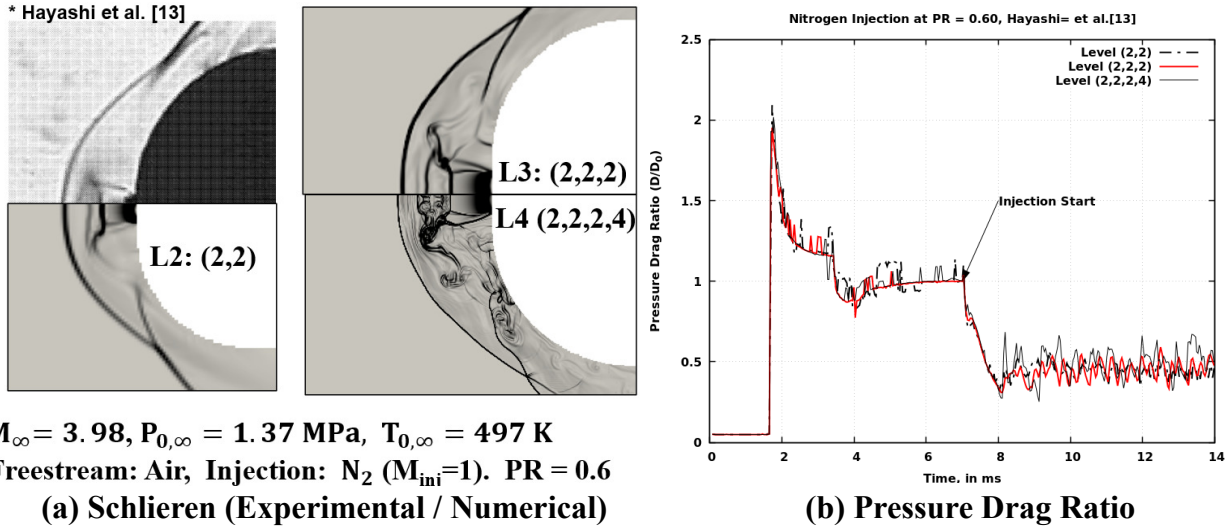

$\mathbf{M_\infty = 3.98, P_{0,\infty} = 1.37\ MPa,\ T_{0,\infty} = 497\ K}$
Freestream: Air, Injection: N_2 (M_{ini}=1). PR = 0.6

(a) Schlieren (Experimental / Numerical) **(b) Pressure Drag Ratio**

Fig. 2 (a) Comparison of numerical and experimental Schlieren images for N_2 injection, the experimental conditions are from Hayashi et al. [13], (b) Time history of Pressure Drag Ratio, for various grid refinement levels.

The grid resolution study for reactive and non-reactive cases have been discussed in this and the next section. In order to qualitatively validate the solver for non-reactive counter-jet flow, one of the experimental cases of sonic counter-jet flow by Hayashi et al. [13], has been simulated. Figure 2a shows the experimental conditions and compares the numerical simulations performed at three different grid refinement levels with experimental Schileren image. A hemispherical blunt nose of diameter 50 mm has been simulated at freestream Mach 3.98 at stagnation pressure and temperature of 1.37 MPa and 487 K, respectively. The nitrogen gas has been injected from 2 mm diameter hole at sonic speed ($M_j = 1$) and stagnation pressure ratio ($P_{j,0}/P_{0,\infty}$) = 0.60. In this case the simulation is performed for total 14 ms and nitrogen is injected at 7 ms time. The computed pressure drag was non-dimensionalized by the computed drag of blunt nose without drag control (D_0) and it had been plotted in Fig. 2b. The three different levels of grid adaptations are used as (2,2), (2,2,2) and (2,2,2,4), which are representing the minimum grid size of 0.50mm, 0.25 mm and 0.0625. The plot reflects the unsteady flow behaviour from impulse start at $t = 0$ to stable bow-shock formation. At $t = 7$ ms, the drag will reduce because of starting of counter-jet flow, which fluctuates and remain unsteady for rest of the time-duration. The numerical Schlieren image from coarse grid L2 (2,2) can show the main flow features of counter-jet flow as obtained by Hayashi et al. [13] in short penetration mode (SPM), such as modified frontal bow-shock, barrel shock, Mach disk, reattachment shock. However, medium grid L3 (2,2,2) can also capture fluctuating triple point formed at the interaction of barrel shock and Mach disk. These flow features and associated unsteadiness is finely captured by grid refinement level L4(2,2,2,4) along with shear layer and unsteady re-attachment point. The pressure drag ratio plot fluctuates in similar manner for L3 & L4. The time-averaged drag coefficient (between 10 ms to 14 ms) is less than 2 % between L2 and L3 as well as between L3 and L4.

C. Grid Independence in Reactive Case

In case of reactive gas (hydrogen) injection, it is expected that the injected hydrogen mixes well with the available high pressure air in stagnation zone. The mixing efficiency may depend upon counter-jet penetration length as well as available small scale flow structure near the interface. The highly compressed zone can lead to increase in the temperature of mixture above auto-ignition limit and leads to self-ignition or shock-induced combustion of hydrogen. The flame front will develop behind bow-shock and interact with the shear layer, front bow-shock and the blunt body. Various flow and flame interactions of different space and time scales are expected. The multi-component compressible

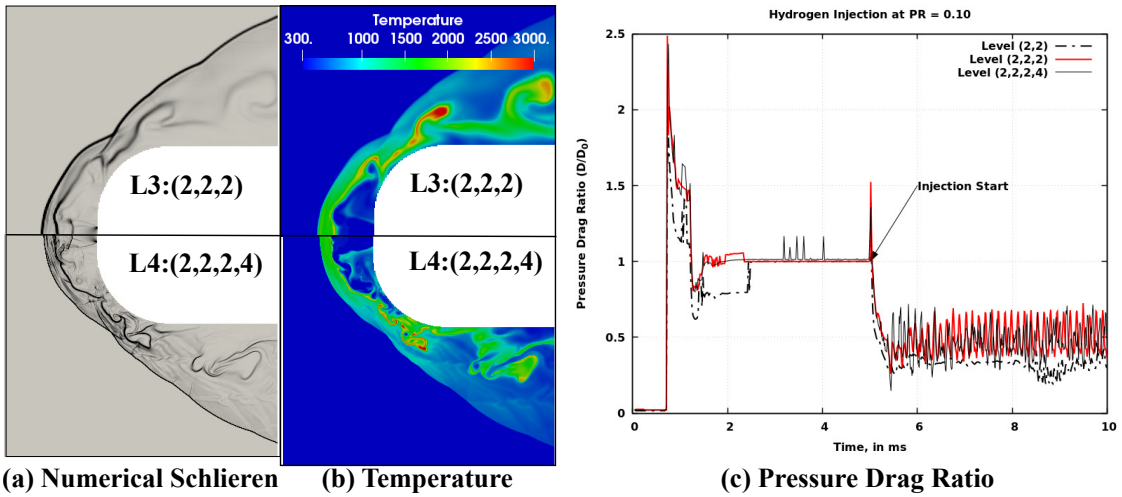

(a) Numerical Schlieren **(b) Temperature** **(c) Pressure Drag Ratio**

Fig. 3 (a) Numerical Schlieren images (b) Temperature and (c) Time history of Pressure Drag Ratio for reactive hydrogen injection in stagnation zone.

Euler solver module in AMROC has already been validated in many previous shock induced combustion, detonation studies. The grid independence study is performed here for reactive case. The same three refinement levels, as previously used for non-reacting case, are simulated for sonic hydrogen injection at 10 % of freestream stagnation pressure. Figure 3 shows the numerical Schlieren, temperature contours and pressure drag ratio plots for medium and fine grid refinement levels. The drag ratio plot shows close trends in L3 (2,2,2) and L4 (2,2,2,4) grid refinements. The difference in time-averaged pressure drag ratio is less than 2 % between L3 and L4. The numerical Schlieren for L3 refinement levels, captures various flow features as well as the flame front between the Mach disk and the frontal shock, which becomes slightly faded behind the re-attachment point. The numerical Schlieren image obtained from the simulation of grid refinement level L4 (2,2,2,4) captures flow features sharply between frontal shock and blunt body along with the interaction of flame front and blunt nose near the reattachment point. The comparison in temperature plot shows similar major flow features and fine flow structures captured by grid refinement level L4. In order to take care of flow features from non-reactive to reactive cases and making the comparison between them, the grid with refinement level L4 (2,2,2,4) has been selected for all the simulated cases in this study with minimum grid size 0.0625 mm. The minimum grid size here represents 10.6 grid points per induction length l_ig for premixed stoichiometric hydrogen-air mixture at freestream condition, which should be sufficient to capture any local detonation phenomenon. However, it may also be necessary to use detailed chemical kinetics in order to capture proper detonation structure with resolution of induction length and if the local detonation may exist. Overall, the selected grid refinement L4 (2,2,2,4) will provide adequate resolution for the objectives of current parametric study.

III. Results and Discussions

The performance of a counter-jet flow on drag reduction depends on various operating parameters such as mass flow rate of injecting gas ($\dot{m}_j$), stagnation pressure ratio of injecting jet and freestream flow (PR) and momentum ratio of incoming jet and freestream jets (R_{MA}) [15, 25]. These parameters are defined as:

$$\dot{m}_j = \rho_j V_j A_j \tag{9}$$

$$PR = \frac{P_{0,j}}{P_{0,\infty}} \tag{10}$$

$$R_{MA} = \frac{\rho_j V_j^2 A_j}{\rho_\infty V_\infty^2 A_\infty} \tag{11}$$

where, ρ_j, V_j and A_j represents the density, velocity and exit cross-sectional area for counter-jet flow. $P_{0,j}$ and $P_{0,\infty}$ are stagnation pressures of counter-jet flow and freestream flow, respectively. ρ_∞, V_∞ and A_∞ are freestream density, velocity and cross-section area of blunt nose. The overall drag of blunt nose with counter-jet flow is defined as

summation of aerodynamic drag (pressure + viscous) and opposite thrust generated by counter-jet. In order to achieve effective drag-reduction the momentum ratio (R_{MA}) should be significantly less than 1. If the momentum ratio is higher than 1, it may increase drag, perform deceleration and work as retro-propulsion. In the current study, R_{MA} remains less than 0.063 for sonic and less than 0.12 for supersonic injection cases. The PR has been varied to perform numerical simulations for various sonic ($M_j = 1$) and supersonic ($M_j = 2$) gas injections. The free-stream conditions, blunt nose and counter-jet exit diameter remain same for all the simulations. The counter-jet exit temperature T_j is also kept constant for all the cases as 300 K, hence the exit velocity for sonic or supersonic counter-jet for individual gas (air, helium and hydrogen) will remain constant for respective injection Mach number. The same PR for different gas counter-jet injection will have different density of exit counter-jet flow because of different specific heat ratio (γ_j) and specific gas constant ($R = R_U/w_M$, where R_U is universal gas constant and w_M is molecular weight of individual gas) for air, helium and hydrogen. The lighter the gas, the lesser mass flow rate will be required, while operating at same stagnation pressure ratio (PR). The required mass flow rate for different injecting gas will be proportional to $\sqrt{\gamma_j/R}$ or $\sqrt{\gamma_j w_{M,j}}$ for constant PR. Another important parameter to define the general flow behaviour of counter-jet flow is expansion ratio of counter-jet flow, which can be defined as ratio of static pressure near the central region of stagnation zone after the bow-shock and static pressure at counter-jet exit ($P_{exp} = P_2/P_j$), where P_2 can be computed by assuming a normal shock near the center of bow-shock and P_j can be computed from isentropic relations of jet-exit. The expansion ratio will mainly depends on freestream (M_∞) and jet exit Mach number (M_j) as well as specific heat ratios of freestream gas (γ_∞) and injecting gas (γ_j). The expansion ratio of counter-jet will remain higher than 1 for Mach 1 sonic injection of counter-jet flow, which represents first shock-cell as underexpanded shock structures and short penetration mode (SPM) flow-features of counter-jet flow. However, the expansion ratio less than 1 leads to overexpanded counter-jet flow injection and may exhibit the flow features in long penetration mode (LPM). The supersonic nozzle can only operate at overexpanded jet. Hence, including sonic and supersonic counter-jet will cover both the SPM and LPM modes of counter-jet flow. In the following sections, the sonic injection of air, helium and hydrogen at two $PR = 0.10$ and 0.25 have been simulated and analyzed. The supersonic counter-jet injections of air, helium and hydrogen at Mach 2 have also been simulated and analyzed for $PR = 0.10$, 0.25 and 0.50. The flow-field has been analyzed by numerical Schlieren images based on density gradient. The pressure drag ratio has been analyzed by time-series data and by comparing time-averaged drag coefficient and relative standard deviation for time-dependent fluctuations. Further, the flow features are analysed and compared from the contours for pressure, temperature for air injection, additionally mass fraction of He for helium injection and finally additional contours of mass fractions of hydrogen and water for reactive cases of hydrogen injection.

A. Sonic Gas Injection

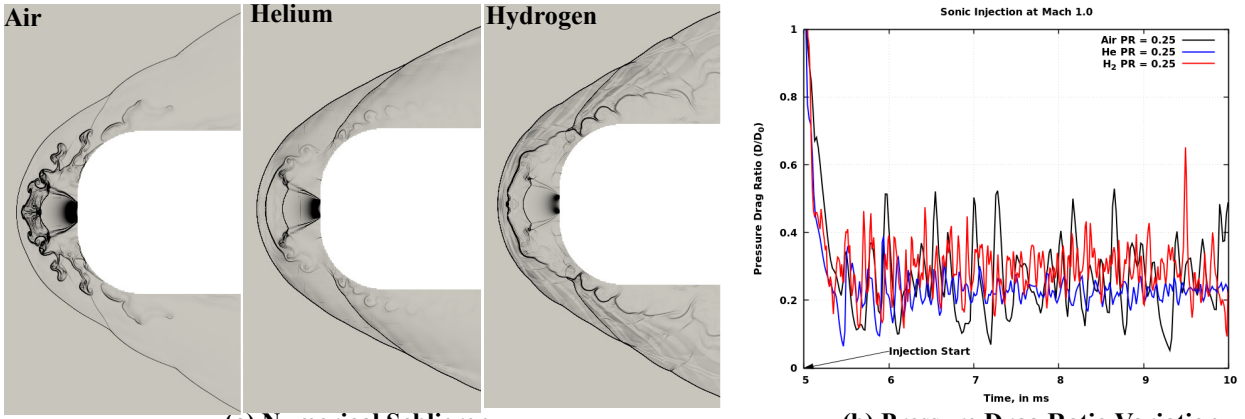

(a) Numerical Schlieren **(b) Pressure Drag Ratio Variation**

Fig. 4 (a) Numerical Schlieren images (b) Variation of Pressure Drag Ratio for sonic air, helium and hydrogen injection at $PR = 0.25$ in SPM

Figure 5 shows various contours for sonic air, helium and hydrogen injections in hypersonic freestream. The non-dimensional pressure (P/P_∞) contours for air injection in Fig. 5a shows high pressure region between the Mach disk and frontal bow-shock near the centerline. In Fig. 5b, the non-dimensional pressure distribution is slightly relaxed

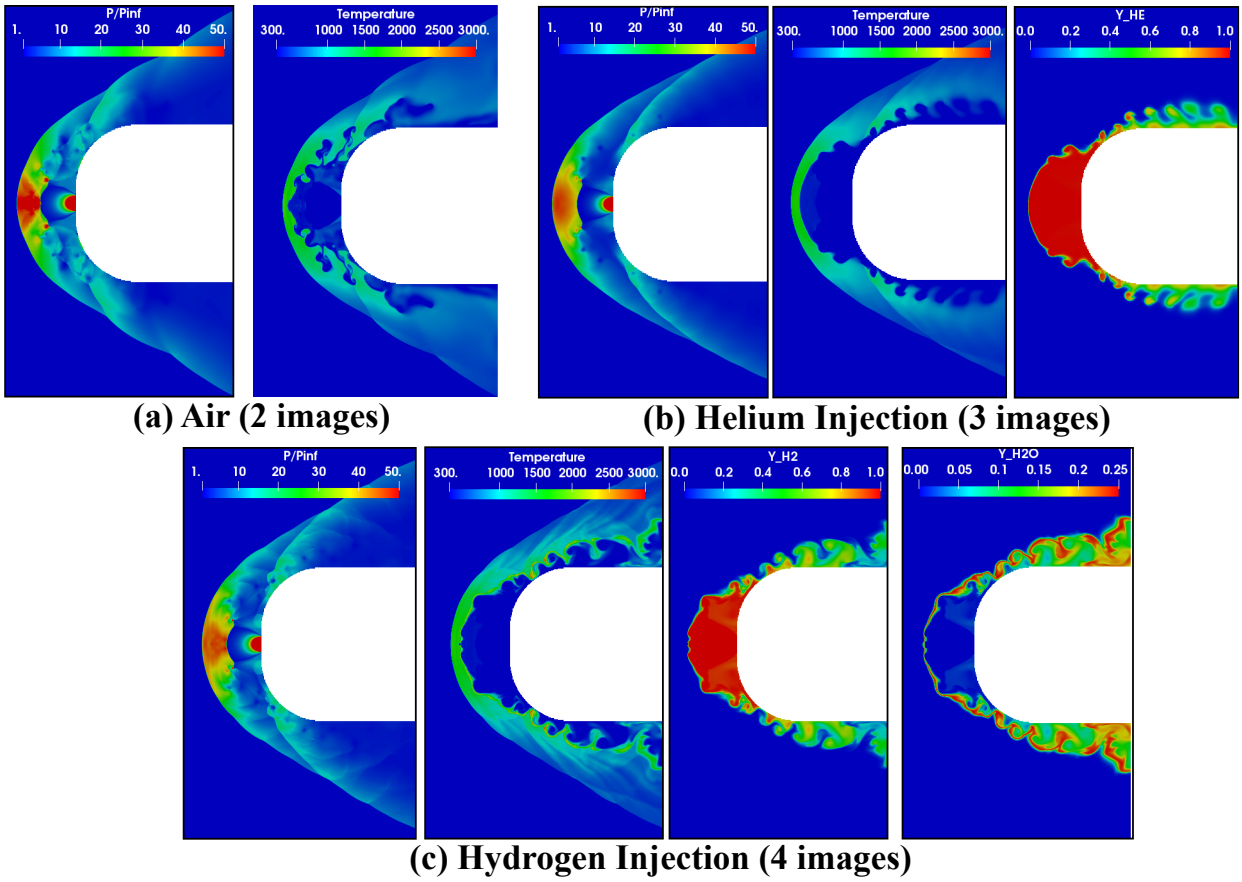

Fig. 5 Various contours for Sonic (a) Air, (b) Helium and, (c) Hydrogen Injection at PR = 0.25 in SPM mode.

Table 1 Performance of Sonic Injection

Injecting Gas	Stagnation Pressure Ratio (PR)	Mass flow ($\dot{m}$) g/s	Pressure Drag Ratio (D/D_0)	Relative Standard Deviation (σ_D/D_0)
Air	0.10	111.8	0.403	0.116
Helium	0.10	41.9	0.395	0.073
Hydrogen	0.10	29.6	0.478	0.091
Air	0.25	279.5	0.270	0.105
Helium	0.25	104.8	0.227	0.023
Hydrogen	0.25	73.9	0.291	0.065

in traverse direction with sonic helium injection. In Fig. 5c, the stagnation flame is present between Mach disk and frontal bow-shock in sonic helium injection case, multiple compression waves can be seen. The temperature variation for non-reactive air, helium injection shows that the high temperature zones are moves away from the blunt nose. In reactive case of hydrogen injection, the flame interacts with the blunt body in downstream zones of shoulder and flat base. Figure 5b shows that the helium completely submerge the blunt nose, while in Fig. 5c, the remaining unburnt hydrogen also submerge the frontal region of blunt nose, but the curved flame-front interacts with the blunt nose. In Fig. 5c, the H_2O mass fraction reflects the completely burnt zone. The thin flame front in the stagnation zone is formed, which grows in thickness and become curved at the downstream locations. Although flame interacts with the blunt nose in downstream region, but the high temperature zones still remain away from the body. It can be seen that various flow features and structure are different with counter-jet flow injection of different gases in the region away from the

blunt nose, but the pressure distribution in the vicinity of the blunt remain almost same which may caused the similar performance of drag reduction for all three sonic injection cases. Table 1 lists down the performance of sonic gas injection at two different stagnation pressure ratios ($PR = 0.10$ and 0.25). The time-averages pressure drag ratios have been calculated between $t = 7$ ms to 10 ms. The relative standard deviation with respect to blunt nose drag (σ/D_0) has also been listed, which reflects the unsteadiness in the flow field. The required input mass flow rates are also listed for comparison. All the three counter-jet flow fields behave in short penetration modes for both PR. The unsteadiness in the flow-field is because of unsteadiness in stagnation interface. At both $PR = 0.10$ and 0.25, sonic helium injection performs comparatively better in pressure drag reduction, also it has lower relative standard deviation. For hydrogen, the pressure drag reduction is higher than air itself for both PR. As hydrogen is lightest gas among three and has specific heat ratio as air, the required mass flow is the lowest (73.5 % less than air) to operate, while helium will be required as 62.5 % less than air. For individual gas injections, the pressure drag reduces with increase in PR, also the relative standard deviation reduces with increase in PR, which means relative unsteadiness in the flow-field reduces.

B. Supersonic Gas Injection

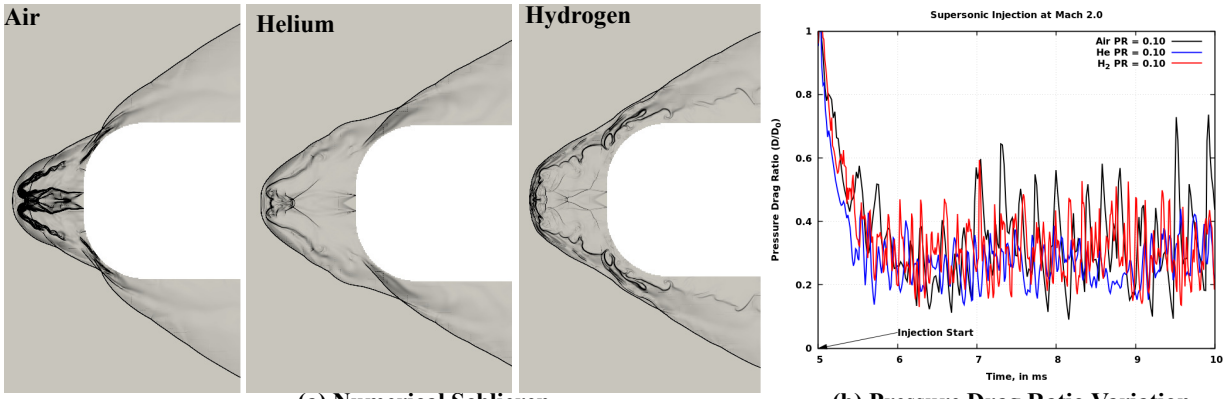

(a) Numerical Schlieren **(b) Pressure Drag Ratio Variation**

Fig. 6 (a) Numerical Schlieren images, (b) Variation of Pressure Drag Ratio for supersonic Mach 2 air, helium and hydrogen injection at PR = 0.10 in LPM

The supersonic Mach 2 injection of air, helium and hydrogen from blunt nose are simulated at three different PR = 0.10, 0.25 and 0.50 in hypersonic freestream of Mach 6. The expansion ratio (P_2/P_j) calculated is 0.48 for air and hydrogen injection with $PR = 0.10$, while it is 0.45 for helium injection at $PR = 0.10$. The counter-jet flow will exit in overexpanded jet manner, which will behave in long penetration mode (LPM) counter-jet flow. The expansion ratio ranges from 1.1 - 1.2 for $PR = 0.25$ gas injections and 2.26-2.4 for $PR = 0.50$. The counter-jet flow operating at $PR = 0.25$ and 0.50 will exit in moderate and highly underexpanded jet, which will exhibit the flow features as short penetration modes (SPM). Figure 6a shows the numerical Schlieren images based on density gradient for supersonic air, helium and hydrogen injection. Figure 6b shows the corresponding drag ratio variation at $PR = 0.10$ for all three gas injection cases after the gas injection time. Based on expansion ratio less than 1, the counter-jet flow will behave as long penetration mode for supersonic injection of all three gases at $PR = 0.10$. The flow-field will remain unsteady in nature as compare to short penetration mode. The frontal bow-shock will be pushed for greater distance. The counter-jet flow in long penetration mode exits as column, with formation of shock cells, but depends on exit pressure and stagnation pressure, the last shock cells near the frontal bow-shock may collapse and form in repetitive manner, which causes higher unsteadiness in the flow field and frontal bow-shock may move higher axial distance than compare to short penetration mode. In Fig. 6a, the supersonic air injection in LPM mode push the frontal bow-shock. The last shock cell bifurcate and there is formation of intermediate reattachment shock between front bow-shock and afterbody shock. The drag ratio plot in Fig. 6b shows higher fluctuations for air injection. In case of helium injection, the frontal bow shock moves higher distance than compare to air injection case. The long column of counter-jet flow can be seen in numerical Schlieren image, however the reattachment shock remains far from shoulder. The drag ratio plot shows least fluctuation for helium injection which indicates that the flow-field may remain stable in comparison to air injection. In case of reactive hydrogen injection in long penetration mode, the frontal shock slightly expanded in transverse direction in comparison to helium injection. The flame front remains close to front shock, which becomes curved at the downstream

locations. The fluctuations in drag ratio plot for supersonic hydrogen injection are higher than the supersonic helium injection.

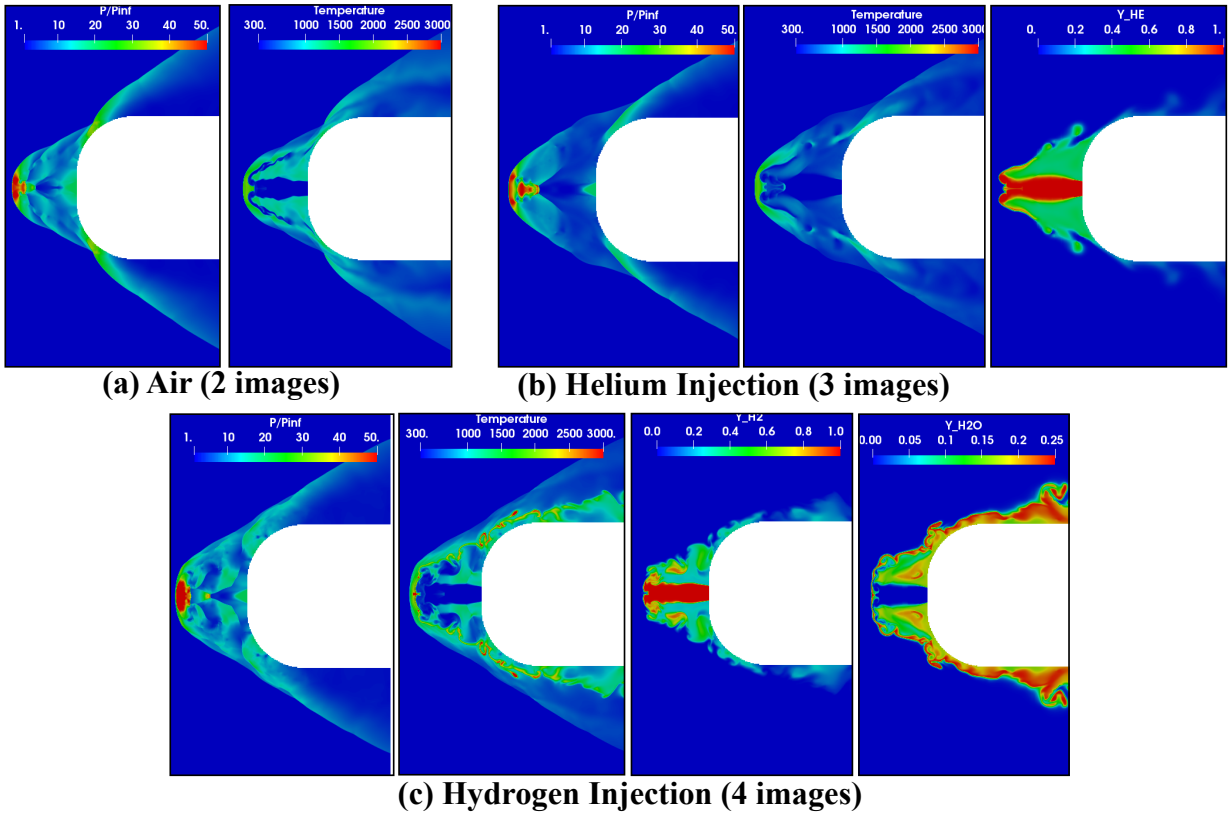

Fig. 7 Various contours for Supersonic Mach 2 (a) Air, (b) Helium and, (c) Hydrogen Injection at PR = 0.10 in LPM mode.

Further Fig. 7 shows various contours for long penetration mode supersonic air, helium and hydrogen injections at $PR = 0.10$. The non-dimensional pressure (P/P_∞) contours in Fig. 7a for air injection shows high pressure zone between frontal shock and near the end of shock cell of counter-jet flow. The reattachment shock in supersonic air injection increases pressure on the shoulder of blunt nose. In case of supersonic helium and hydrogen injections, the non-dimensional pressure (P/P_∞) contours in Fig. 7b and 7c show similar high pressure region near the center of frontal bow shock and end of last shock-cell of counter-jet flow, but has the wider shock envelop, causing reattachment point move away from shoulder for both the cases. The temperature contours for air and helium injection shows how the air column of low temperature penetrates the stagnation nose and after bifurcation near the frontal bow shock makes a shear layer. Similarly in helium injection case, the temperature plot suggests that high pressure stagnation interface may penetrate back to jet column. In Fig. 7c, the central jet column remains unburnt because of unavailability of oxygen on the central region. Behind the frontal bow shock thin stagnation flame region forms, which extends downstream and thickens, but remains curved because of interaction of shear layer. The mass fraction of helium contour in Fig. 7b shows the column of helium and its bifurcation at the end, formation of shear layer. In Fig. 7c, the supersonic hydrogen injection in long penetration mode, leads to better mixing because of available longer axial distance behind the frontal bow shock. The H_2O mass fraction shows thin flame near the center or stagnation interface, but high temperature region forms in front of blunt nose itself, which was not the case in sonic hydrogen injection of short penetration mode. From these contours, it is evident that the frontal bow-shock moves far upstream for helium injection than air or hydrogen. The drag reduction of 72 % is obtained from helium injection at LPM mode, while air and hydrogen injection lead to drag reduction of 65 % and 69 %, respectively.

Figure 8 shows the time-averaged pressure drag ratio plotted for all three stagnation pressure ratios along with relative standard deviation. The increase in PR, leads to reduction in drag ratio for supersonic air injection linearly. However, PR increase in supersonic helium and hydrogen injections first leads to slight increase in pressure drag ratio,

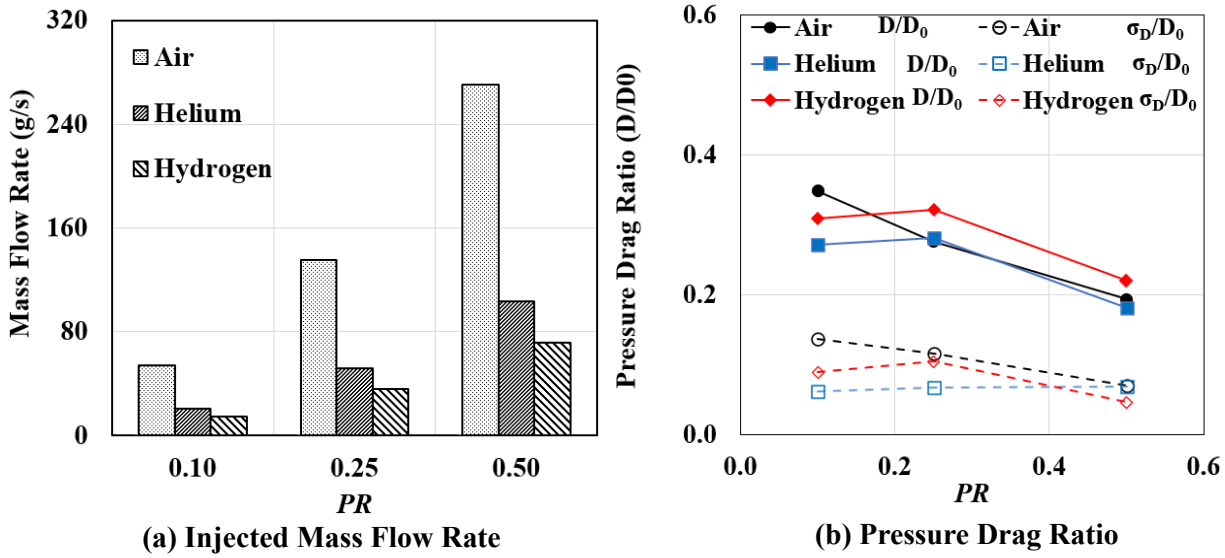

Fig. 8 Supersonic Gas Injection at Mach 2: (a) Required Mass flow rate, (b) Time-averaged Pressure Drag Ratio

but later decrease of the same order as compare to supersonic air injection. The flow field varies from long penetration mode to short penetration mode, which may cause slight different behaviour between light and heavier gas. The flow features of short penetration mode remain similar to sonic injection, hence are not discussed here. The supersonic hydrogen injection shows higher pressure drag ratio than helium for all PR. The performance of helium and air remain similar in short penetration mode. The best drag reduction of 81-82 % is found in case of supersonic air and helium injection. The flow unsteadiness reduced linearly for supersonic air injection with increase in PR, while PR increase in supersonic helium injection leads to slightly increase in unsteadiness. In case of hydrogen injection, the unsteadiness slightly increases initially with increase in PR 0.10 to 0.25, but reduces below air and helium at higher PR. Fig. 8a shows the requires mass flow rate for individual supersonic gas injection. The requirement of hydrogen injection is far less than air injection requirement and requirement of mass flow rate of supersonic helium injection is higher than hydrogen, but still far less than air requirement for same PR. When comparing same PR for sonic and supersonic gas injection, the requirement of mass flow rate is lesser in case of supersonic injection and the performance is also better in supersonic gas injection. In the current study, the formation of local detonation was not observed in case of reactive gas injection in non-premixed manner. Also, there is no intermittent SPM and LPM mode observed in reactive gas injection cases as observed by Vashishtha et al.[15]. It may be possible that Mach number of jet may play important role in increasing the penetration length and possibility of detonation initiation. In furture work the effect of Mach number will be studied to achieved detonation initiation while injecting in stagnation zone. Also, it may also be important to utilize detailed chemistry for the reactive hydrogen injection cases.

IV. Conclusions

In an attempt to investigate the effect of light gas injection in stagnation zone on the drag reduction, the numerical simulation are performed to simulate the sonic and supersonic direct gas injection in a stagnation zone of blunt nose at freestream hypersonic flow of Mach 6. The two-dimensional axisymmetric unsteady compressible multi-component Euler equations are solved by using structured block adaptive mesh refinement with AMROC solver. The sonic counter-jet flow injection of light non-reactive gas helium shows stable short penetration mode and best performance in drag reduction up to 77 %, while air injection at same stagnation pressure ratios shows highly fluctuating short penetration mode because of unstable stagnation interface between Mach disk and modified front bow-shock. In case of sonic counter-jet injection of light reactive gas, hydrogen at simulated stagnation pressure ratio, undergo shock induced combustion and thin stagnation flame front forms between frontal shock and Mach disk. The flame front becomes curved and thick in downstream locations and interacts with reattachment shock causes increase in fluctuation in drag ratio plots. The required mass flow rate for light gas injection to get similar or better performance in drag reduction in

sonic injection cases are 72.5 % and 62.5 % for hydrogen and helium gases, respectively in comparison to air. This lesser requirement only depends on gas properties at constant stagnation pressure ratio (PR). In case of supersonic counter-jet injection at hypersonic Mach 6, the performance of inert gas helium injection on drag reduction is similar to air injection at $PR = 0.25$ and 0.5, while the reactive gas injection provides lower drag reduction than air injection. It can be because of energy addition by hydrogen injection near the blunt body in short penetration mode. At $PR = 0.10$, all three gas injection exhibit long penetration mode counter flow jet. The counter-jet injection of both the light gases show the higher drag reduction up to 82 %in comparison to air injection as well as better stability than the air injection. The requirement of mass flow rate for light gas injection at constant PR are lesser in the same proportion as sonic injection in comparison to air. In the current simulations of direct reactive gas injection in stagnation zone, shows only deflagaration mode combustion. There was no detonation mode observed for studied operating conditions. The current simulation employs high resolution grid and solves Euler equation for mixing problem of non-premixed gas injection. In the current set-up, the mixing is governed by vorticity and numerical diffusion in absence of physical viscosity. In the high-resolution zones the numerical diffusion becomes smaller. Hence the next logical step will be to incorporate the physical diffusion correctly by solving the Navier-Strokes equations. On the other hand, further parametric studies will be useful to enhance mixing of injecting gas in stagnation zone to obtain detonation initiation.

Acknowledgments

The authors would like to acknowledge and thank the Enterprise Research and Incubation Centre (ERIC) at Institute of Technology Carlow for providing access to the computing resources for this study.

References

[1] Ahmed, M. Y., and Qin, N., "Forebody shock control devices for drag and aero-heating reduction: A comprehensive survey with a practical perspective," *Progress in Aerospace Sciences*, Vol. 112, 2020, p. 100585. https://doi.org/10.1016/j.paerosci.2019.100585.

[2] Vashishtha, A., and Khurana, S., "On Unsteady Flow Analysis of a Round Spike Blunt Nose Afterbody in Mach 6 Flow," *IOP Conference Series: Materials Science and Engineering*, Vol. 1024, No. 1, 2021, p. 012017. https://doi.org/10.1088/1757-899x/1024/1/012017.

[3] Vashishtha, A., and Khurana, S., "Pulsating Flow Investigation for Spiked Blunt-Nose Body in Hypersonic Flow and its Control," *AIAA Scitech 2021 Forum*, AIAA 2021-0839, 2021. https://doi.org/10.2514/6.2021-0839.

[4] Vashishtha, A., and Rathakrishnan, E., "Breathing blunt-nose concept for drag reduction in supersonic flow," *Proceedings of the Institution of Mechanical Engineers, Part G: Journal of Aerospace Engineering*, Vol. 223, No. 1, 2009, pp. 31–38. https://doi.org/10.1243/09544100JAERO369.

[5] Watanabe, Y., Suzuki, K., and Rathakrishnan, E., "Aerodynamic characteristics of breathing blunt nose configuration at hypersonic speeds," *Proceedings of the Institution of Mechanical Engineers, Part G: Journal of Aerospace Engineering*, Vol. 231, No. 5, 2017, pp. 840–858. https://doi.org/10.1177/0954410016643979.

[6] Vashishtha, A., Watanabe, Y., and Suzuki, K., "Study of Shock Shape in front of Concave, Convex and Flat Arc in Hypersonic Flow," *JAXA Special Publication*, Vol. JAXA-SP-14-010, Japan Aerospace Exploration Agency JAXA, 2015, pp. 127–132. URL http://id.nii.ac.jp/1696/00003852/.

[7] Vashishtha, A., Watanabe, Y., and Suzuki, K., "Study of Bow-Shock Instabilities in front of Hemispherical Shell at Hypersonic Mach Number 7," *45th AIAA Fluid Dynamics Conference*, AIAA 2015-2638, 2015. https://doi.org/10.2514/6.2015-2638.

[8] Vashishtha, A., Watanabe, Y., and Suzuki, K., "Bow-Shock Instability and its Control in front of Hemispherical Concave Shell at Hypersonic Mach Number 7," *Transaction of the JSASS, Aerospace Technology Japan*, Vol. 14, No. ists30, 2016, pp. 121–128. https://doi.org/10.2322/tastj.14.Pe_121.

[9] Joarder, R., "On the mechanism of wave drag reduction by concentrated laser energy deposition in supersonic flows over a blunt body," *Shock Waves*, Vol. 29, 2019, pp. 487–497. https://doi.org/10.1007/s00193-018-0868-3.

[10] Azarova, O., and Knight, D., "An approach of drag force decrease for combined cylinder AD bodies under the action of microwave and laser energy deposition," *Aerospace Science and Technology*, Vol. 64, 2017, pp. 154–160. https://doi.org/10.1016/j.ast.2017.01.025.

[11] Satheesh, K., and Jagadeesh, G., "Experimental investigations on the effect of energy deposition in hypersonic blunt body flow field," *Shock Waves*, Vol. 18, 2008, pp. 53–70. https://doi.org/10.1007/s00193-008-0140-3.

[12] Warren, C. H. E., "An experimental investigation of the effect of ejecting a coolant gas at the nose of a bluff body," *Journal of Fluid Mechanics*, Vol. 8, No. 3, 1960, p. 400–417. https://doi.org/10.1017/S0022112060000694.

[13] Hayashi, K., and Aso, S., "Effect of Pressure Ratio on Aerodynamic Heating Reduction due to Opposing Jet," *36th AIAA Thermophysics Conference*, 2003. https://doi.org/10.2514/6.2003-4041.

[14] Korzun, A. M., Braun, R. D., and Cruz, J. R., "Survey of Supersonic Retropropulsion Technology for Mars Entry, Descent, and Landing," *Journal of Spacecraft and Rockets*, Vol. 46, No. 5, 2009, pp. 929–937. https://doi.org/10.2514/1.41161.

[15] Vashishtha, A., Callaghan, D., and Nolan, C., "Drag Control by Hydrogen Injection in Shocked Stagnation Zone of Blunt Nose," *IOP Conference Series: Materials Science and Engineering*, Vol. 1024, No. 1, 2021, p. 012110. https://doi.org/10.1088/1757-899x/1024/1/012110.

[16] Shang, J. S., Hayes, J., Wurtzler, K., and Strang, W., "Jet-Spike Bifurcation in High-Speed Flows," *AIAA Journal*, Vol. 39, No. 6, 2001, pp. 1159–1165. https://doi.org/10.2514/2.1430.

[17] Rankin, B. A., Richardson, D. R., Caswell, A. W., Naples, A. G., Hoke, J. L., and Schauer, F. R., "Chemiluminescence imaging of an optically accessible non-premixed rotating detonation engine," *Combustion and Flame*, Vol. 176, 2017, pp. 12–22. https://doi.org/10.1016/j.combustflame.2016.09.020.

[18] Deiterding, R., "Parallel adaptive simulation of multi-dimensional detonation structures," Ph.D. thesis, Brandenburgische Technische Universität Cottbus, 2003. URL http://rdeiterding.website/pub/thesis_us.pdf.

[19] Deiterding, R., "High-Resolution Numerical Simulation and Analysis of Mach Reflection Structures in Detonation Waves in Low-Pressure H_2–O_2–Ar Mixtures: A Summary of Results Obtained with the Adaptive Mesh Refinement Framework AMROC," *Journal of Combustion*, Vol. 2011, 2011, p. 738969. https://doi.org/10.1155/2011/738969.

[20] Deiterding, R., "A parallel adaptive method for simulating shock-induced combustion with detailed chemical kinetics in complex domains," *Computers & Structures*, Vol. 87, No. 11, 2009, pp. 769–783. https://doi.org/10.1016/j.compstruc.2008.11.007, fifth MIT Conference on Computational Fluid and Solid Mechanics.

[21] Liang, Z., Browne, S., Deiterding, R., and Shepherd, J., "Detonation front structure and the competition for radicals," *Proceedings of the Combustion Institute*, Vol. 31, No. 2, 2007, pp. 2445–2453. https://doi.org/10.1016/j.proci.2006.07.244.

[22] R. J. Kee, F. M. R., and Miller, J. A., "Chemkin-II: A Fortran chemical kinetics package for the analysis of gas-phase chemical kinetics," Tech. rep., SAND89-8009, Sandia National Laboratories, Livermore, California, 1989.

[23] R. J. Kee, F. M. R., and Miller, J. A., "The Chemkin thermodynamic data base," Tech. rep., SAND87-8215B, Sandia National Laboratories, Livermore, California, 1990.

[24] ChangJian Wang, S. L., Jennifer Wen, and Guo, J., "Single-step chemistry model and transport coefficient model for hydrogen combustion," *Sci. China Technol. Sci.*, Vol. 55, 2012, pp. 2163–2168. https://doi.org/10.1007/s11431-012-4932-4.

[25] Desai, S., Prakash K, V., Kulkarni, V., and Gadgil, H., "Universal scaling parameter for a counter jet drag reduction technique in supersonic flows," *Physics of Fluids*, Vol. 32, No. 3, 2020, p. 036105. https://doi.org/10.1063/1.5140029.